Amri, A., Jiang, Z-T, Zhao, X., Xie, Z., Yin, C-Y, Ali, N., Mondinos, N., Mahbubur Rahman, M. and Habibi, D. (2014) Tailoring the physicochemical and mechanical properties of optical copper–cobalt oxide thin films through annealing treatment. Surface and Coatings Technology, 239. pp. 212-221.

Tailoring the physicochemical and mechanical properties of optical copper cobalt oxide thin films through annealing treatment

Amun Amri, Zhong-Tao Jiang, Xiaoli Zhao, Zonghan Xie, Chun-Yang Yin, Nurshahidah Ali, Nick Mondinos, M. Mahbubur Rahman, Daryoush Habibi

PII: S0257-8972(13)01136-5
DOI: doi: 10.1016/j.surfcoat.2013.11.044
Reference: SCT 19038

To appear in: *Surface & Coatings Technology*

Received date: 11 July 2013
Accepted date: 8 November 2013

Please cite this article as: Amun Amri, Zhong-Tao Jiang, Xiaoli Zhao, Zonghan Xie, Chun-Yang Yin, Nurshahidah Ali, Nick Mondinos, M. Mahbubur Rahman, Daryoush Habibi, Tailoring the physicochemical and mechanical properties of optical copper cobalt oxide thin films through annealing treatment, *Surface & Coatings Technology* (2013), doi: 10.1016/j.surfcoat.2013.11.044

Tailoring the physicochemical and mechanical properties of optical copper cobalt oxide thin films through annealing treatment

Amun Amri[a,e] , Zhong-Tao Jiang[a,*] , Xiaoli Zhao[b], Zonghan Xie[b,c], Chun-Yang Yin[d,*], Nurshahidah Ali[a], Nick Mondinos[a], M. Mahbubur Rahman[a], Daryoush Habibi[b]

[a]*School of Engineering and Information Technology, Murdoch University, Murdoch, 6150 WA, Australia*

[b]*School of Engineering, Edith Cowan University, Joondalup, WA 6027, Australia*

[c]*School of Mechanical Engineering, University of Adelaide, SA 5005, Australia*

[d]*Chemical and Analytical Sciences, Murdoch University, Murdoch, 6150 WA, Australia*

[e]*Department of Chemical Engineering, Riau University, Pekanbaru 28293, Indonesia*

*Corresponding author. Tel.: +618 9360 2867; Email address: Z.Jiang@murdoch.edu.au

*Tel.: +614 3140 9216; Email address: C.Yin@murdoch.edu.au

Abstract

Sol-gel dip-coated optical coatings, copper-cobalt oxides on aluminium substrates, were thermally treated at different annealing temperatures in the range 500 – 650 °C. The resulting films were characterized using X-ray diffraction (XRD), X-ray photoelectron spectroscopy (XPS), UV-Vis-NIR spectrophotometry and nanoindentation techniques. The crystallinity of $CoCu_2O_3$ enhanced significantly, with increasing annealing temperature from 500 to 650 °C, while the electronic structure and bonding states of the copper-cobalt oxides matrix remained unchanged. UV-Vis-NIR analysis showed that the solar absorptance (α) of the coatings changed with increasing of annealing temperature and an optimum α (84.4%) was achieved at 550 °C, which also coincides to the maximum tensile residual stress of the coating. Nanoindentation tests exhibited an increasing trend in both the hardness (H) and elastic modulus (E) of the coatings with increase in annealing temperature, although a slight decrease in the H/E ratio was also observed. The experimental studies were complemented by Finite Element Modelling (FEM). The results showed that, under mechanical loading, the stress and plastic deformation were concentrated within the coating layers. As such, the likelihood of delamination of the coating layer upon unloading would be reduced.

Keywords: *Thin film coating; annealing; copper cobalt oxides; solid state ionics; finite element modelling*

1. Introduction

Copper cobalt oxides are a family of metal oxides which have found important applications in electro-catalytic reactions and as thermoelectric material [1-13]. To enable improved designs for optimal performance in these applications, their physicochemical, electrochemical, magnetic, conductivity as well as thermal properties have been intensely studied, in conjunction with their structural characteristics [6, 8, 13-16]. From these previous studies, it can be construed that temperature change in the synthesis process or application has substantial influence on their physicochemical properties.

The temperature effect on the structural, magnetic and electronic structure properties in the delafossite-type of copper cobalt oxides were established [13]. The thermal analysis showed the compounds are stable up to 680°C, whereupon a phase transition event occurs. A weak temperature dependent magnetic susceptibility exists, which remains negative in the temperature range from ~20 K to 300 K. There is no ferromagnetic or paramagnetic impurity contribution from samples at temperatures as low as 2 K [13]. The temperature independent diamagnetism reported for this type of copper cobalt oxide is in agreement with formal charge assignments of Cu^{+} (d^{10}) and Co^{3+} (d^{6}, low spin) as suggested by Shannon *et al.* [17] as well as from analysis of the electronic band structure determined by density functional theory (DFT) calculations [12, 13]. The spinel-type of copper cobalt oxides tends to form a low crystallized single phase of copper cobalt oxide with a partially inverted spinel structure and minor segregations of new cobalt and/or copper oxide phases, which depend on the Cu/Co ratio in the precursor salt as well as the calcination temperature [8, 18]. The increase of calcination temperature is typically accompanied by an increase in the degree of crystallinity of phases in copper cobalt oxides [16]. Nonetheless, the opposite result was observed by Shaheen [16], where the degree of crystallinity of detected phase in copper cobalt oxide decreased when synthesized by lower content of copper in Cu/Co ratio. Indeed, this discrepancy can be

addressed by considering the dissolution of more cobalt species in the lattice of the copper cobaltite phase, thus producing a more homogeneous solid solution [16].

Compared to the above mentioned properties, the mechanical properties of optical copper cobalt mixed oxides are seldom studied and, to the best of our knowledge, there is no integrated experimental and modelling study on the mechanical properties of copper cobalt oxides coatings. This is quite surprising, in view of the fact that mechanical strength and durability are important in extending their service life. In our previous work, the copper cobalt oxide thin films were deposited on aluminium substrate *via* the sol-gel dip-coating route [19, 20, 21]. The resulting coatings exhibited distinctive optical properties with a spectrally selective profile in the UV-Vis-NIR wavelengths region. There are, however, still many unresolved engineering issues, especially those as regards to the understanding of the influence of annealing temperatures on the physicochemical and mechanical properties of the coatings. Therefore, the aim of this work is to investigate the structural, surface compositions, optical and mechanical properties of copper cobalt oxide thin film coatings synthesized at different annealing temperatures using XRD, XPS, UV-Vis-NIR and nanoindentation. Moreover, the experimental results are used to evaluate the mechanical behaviour of the coatings by Finite Element Modelling (FEM). The high absorptance value accompanied by the high mechanical robustness of the copper cobalt oxide coating renders these coatings a promising material for various applications, especially for solar selective absorption.

2. Experimental

2.1. Preparation of thin film coatings

Copper-cobalt oxide thin film coatings were deposited using a sol-gel dip-coating technique described in our previous reports [19, 20] with some variations as elucidated in the following. Copper (II) acetate monohydrate ($Cu(OOCCH_3)_2.H_2O$, Alfa Aesar, 98 %), Cobalt (II) chloride ($CoCl_2.6H_2O$, APS Chemical, > 99 %), propionic acid (C_2H_5COOH, Chem

Supply, 99 %) and absolute ethanol (Merck) were used as received. Commercial aluminium (Anofol, size: 2×4 cm^2) was used as substrate. The copper and cobalt precursors (at 0.25 M for each) were mixed using absolute ethanol. Propionate acid was then added to the solution as complexing agent and stirred for 2 hours. The resulting solution was then used for deposition on aluminium substrates using a dip-coater at a withdrawal rate of 120 mm/min with relative humidity being controlled below 55%, and subsequently heated on a hot plate at 150°C for 10 seconds. The dip-heating cycles were conducted four times before final annealing at temperatures from 500°C to 650°C for 1 hour. Four dip-heating cycles process was adopted because it could provide an optimized reflective system compared to other numbers of cycles [20]. If the annealing temperature was set lower, residual organic groups would not be completely removed, while temperatures higher than 650°C could also not be applied since it was limited by the melting point of aluminium substrate. The ramp-rates of 50°C/min was selected for the heating process before reaching the final annealing temperatures, while cooling to room temperature was allowed to occur naturally inside the closed furnace.

2.2. Characterizations

Mineralogical characteristics of the thin films were analyzed using a X-Ray Diffractometer (Bruker Advance D8 X-Ray Diffractometer) equipped with a Lynx-Eye detector, Cu-tube and operated at 40 kV and 40 mA [22]. Conditions of analysis were set as follows: 15 rpm rotation, 10-60° of 2θ, 0.01 degree increment, 1.2 sec/step-time per step, 0.26 degree fixed divergence slit and 2.20 degree fixed anti-scatter slit. The surface bonding structures of samples were probed by X-ray photoelectron spectroscopy (XPS) (Kratos Axis Ultra XPS spectrometer, Manchester, UK) with Al K_α radiation (hv=1486.6 eV) [23]. The samples were mounted horizontally on the holder and normal to the electrostatic lens, using double-sided Cu sticky tape. The vacuum pressure of the analyzer chamber was less than 10^{-9} Torr. The voltage and emission current of the X-ray source were held at 12 kV and 12 mA, respectively.

Initial survey scans used a pass energy of 80 eV. To ensure a high resolution and good sensitivity for the features of interests, a pass energy of 10 eV was used. The XPS spectra energy scale was calibrated using Cu *2p* (932.67 eV), Ag *3d* (368.27 eV), C *1s* (284.8 eV; hydrocarbon: C–H) and Au *4f* (83.98 eV). The electrostatic lens mode and analyzer entrance of the XPS instrument were selected using the Hybrid and Slot mode (iris=0.6 and aperture=49), respectively. Charge neutralization was employed during the XPS measurements. Surfaces of the samples were cleaned by etching with Ar^+ for about 2 minutes when the O *1s* and C *1s* intensities reached minimum. The total sample current and Ar^+ gun emission current were 75nA and 15mA, respectively. The gun acceleration voltage was 4.5 kV. The base pressure of the sample analysis chamber was at about 10^{-10} Torr and the working pressure with high purity Ar^+ gas for etching was 3×10^{-8} torr. The CASA XPS (V.2.3.15) software was utilized for quantification analysis with Shirley background subtraction. The solar absorptance was calculated based on the AM1.5 solar spectrum standard [24] using the near normal hemispherical reflectance from 300 to 2700 nm recorded by a UV–Vis-NIR Jasco V-670 double beam spectrophotometer with an integrating sphere.

A nanoindentation workstation (Ultra-Micro Indentation System 2000, CSIRO, Sydney, Australia) equipped with a Berkovich indenter [25, 26] was used to determine the mechanical properties of the films. To ensure that only the film properties were measured, nanoindentation was conducted under load control with a maximum load of 0.5 mN, under which the maximum penetration depth was found to be ~0.1 μm (see Results and discussion section), well below 10% of the total film thickness of ~2 μm. For each test, 10 incremental and 10 decremental steps were used, respectively. For each sample, 30 measurements were taken. The results were then averaged and the standard deviation was evaluated for each sample. Finite element modelling (FEM) was used to assess the mechanical response of the coating system to external loadings. Input parameters consisted of both structural and mechanical properties of the coating systems obtained from experiments. A two-dimensional

(2D) axisymmetric model was constructed with the loading direction along the axial *z* axis, using COMSOL software. The details of the model set-up are given in our previous work [27, 28], and are briefly described below. The model assembly comprises a coating (1 μm thick) placed on top of aluminium substrate (49 μm thick), loaded under a spherical tipped indenter with a radius of 5 μm. The simulation block is a rectangle measuring 50 × 50 μm. The coating is assumed to be bonded perfectly to the substrate. Time-dependent deformation behaviours such as creep, as well as surface roughness and contamination, were not considered in our simulations. The contact between the indenter and the sample was assumed to be frictionless. The bottom of the simulation model (z = 50 μm) was fixed in the z direction, while the right edge of the block (x = 50 μm) was fixed in the x direction. The axisymmetric axis coincided with the left edge of the simulation block (x = 0), as such, 3D effects could eventually obtained. The tip of the indenter was located at z = 0 μm at the beginning of the simulation. The indentation loading process was simulated as downward movements in successive steps of 0.01 μm each, starting from 0 to 0.12 μm.

3. Results and Discussion

3.1. XRD analysis

XRD patterns of coated samples synthesized on aluminium substrates and treated at different annealing temperatures are shown in Fig. 1. Analyses of peak intensities and *d*-spacing for peaks in the regions of 35.3° (0 1 1), 36.9° (3 1 0) and 40.2° (3 0 1) assigned the phase to $CoCu_2O_3$ (ICDD 76-0442) and in agreement with the orthorhombic crystal system (Space Group = Pmmn [#59]). The peaks at approximately 31.3° and 38.5° can be attributed to mixed phases of $CoCuO_2$ (ICDD 74-1855) and $CuCoO_2$ (ICDD 21-0256). The crystallinity along the (301) direction of $CoCu_2O_3$ increases with higher annealing temperature.

Analysis of domain size from the (310) and (301) peaks using the Debye-Scherrer formula (equation 1) is tabulated in Table 1. The results indicate that as the annealing temperature

increases, the domain measured perpendicular to the (3 1 0) lattice plane increases significantly, while the domain measured perpendicular to the (3 0 1) plane decreases slightly.

$$t_{hkl} = \frac{K\lambda}{B\cos\theta_B} \quad (1)$$

where K is the crystallite-shape factor (K=0.94 [29-31]); B=$FWHM$.

It has been established that, the strain within a material can be evaluated by measuring the d-spacing of the crystal planes using X-ray diffraction [32]:

$$\varepsilon_z = (d_n - d_0)/d_0 \quad (2)$$

where ε_z is the strain component normal to the surface, d_0 and d_n are the strain free and measured d-spacing, respectively. Within a coating layer of ~1 μm thickness, the residual stress σ_z is normally zero [33]. As such, we have [34]:

$$\varepsilon_z = -\nu(\varepsilon_x + \varepsilon_y) = -(\nu/E)(\sigma_x + \sigma_y) \quad (3)$$

where ν is Poisson's ratio, E is Young's modulus, σ_x and σ_y are the in-plane principal stresses along the x and y directions, respectively. Combining Equation (2) and (3), and assuming that the coating layer is isotropic, *i.e.*, $\sigma_x = \sigma_y$, we obtain:

$$2\sigma_x = -(E/\nu)(d_n - d_0)/d_0 \quad (4)$$

from which the in-plane residual stress within the $CoCu_2O_3$ phase can be estimated. The E values were obtained from first principles calculations (*i.e.*, 85 GPa along (3 0 1) and 122 GPa along (3 1 0), respectively). Although these results may not directly represent the stress levels within the coatings, they, nonetheless, provide an evaluation of the trend in stress changes due to different annealing temperatures. It is also interesting to note that the average E value within the coatings obtained from our nanoindentation results (*i.e.*, 100 GPa, see Section 3.4) is in general agreement with those derived from first principles calculations, indicating that the actual stress level within the coatings may be close to those obtained from the above calculations. By bearing this in mind, the residual stress was found to decrease with the

annealing temperature; that is, from 500 to 650°C, the tensile residual stress reduced by ~48% (Table 2).

3.2. XPS study

Fig. 2 and Fig. 3 show the Cu *2p* XPS spectra and the decoupling of Cu $2p_{3/2}$ peaks of copper cobalt oxide film coatings synthesized at different annealing temperatures, respectively. In every spectrum, the two main peaks of Cu $2p_{3/2}$ and Cu $2p_{1/2}$ and the satellites on the high energy side of these two main peaks can be found (Fig. 2). Qualitatively, in every spectrum, the binding energy difference between Cu $2p_{1/2}$ and Cu $2p_{3/2}$, which is around 19.8 eV, indicates the presence of a low oxidation state of copper, while the satellite peak between Cu $2p_{3/2}$ and Cu $2p_{1/2}$ confirms the presence of Cu^{2+}. It is widely established that this satellite arises due to the shake-up transition by a ligand metal *3d* charge transfer that does not occur with Cu^{+} species which have completely filled *3d* shells. From Fig. 2, it can be seen that the Cu $2p_{3/2}$ satellite intensity to Cu $2p_{3/2}$ main peak intensity ratio (I_{sat}/I_{main}) varies slightly from 0.1 to 0.15 as the annealing temperature is increased from 500 to 650 °C, indicating that there is a decrease in the covalent character of the Cu-O bond in copper cobalt mixed oxide [18].

The decoupling of Cu $2p_{3/2}$ peak and its satellite in every coating is shown in Fig. 3.a-d. Overall, the curve-fittings result in four components in every spectrum and they are quantified in Table 3. It is commonly recognized that the photoelectron peak at around 932.3-932.4 eV of Cu $2p_{3/2}$ is usually from the tetrahedral Cu^{+}. The components at around 933-934 eV with their satellites characteristic are due to the octahedral Cu^{2+}. From Table 3, it can be seen that the tetrahedral Cu^{+} ions remain more prominent compared to the octahedral Cu^{2+} ions, even though the annealing temperature is increased. The increase of annealing temperature generally does not change the copper bonding structure in the surface. The absence of a component at the low energy side of the Cu $2p_{3/2}$ peak indicates that natural cooling overnight to room temperature inside the closed oven furnace might prevent the reduction of octahedral

Cu^{2+} in contrast to the relatively faster cooling outside the furnace as reported in our previous work [20].

Fig. 4 shows the profile of Co *2p* spectra for samples synthesized at different annealing temperatures. Similarly, in every spectrum, the two main peaks can be attributed to Co $2p_{3/2}$ and Co $2p_{1/2}$ and the satellites are located in the high energy sides of these two main peaks. Qualitatively, the Co $2p_{3/2}$ and Co $2p_{1/2}$ peaks separated by a spin-orbit splitting of ~15.9 eV and the Co $2p_{1/2}$ to Co $2p_{3/2}$ intensities ratio of 0.5 correspond to the Co^{2+} ions [35]. The presence of a characteristic satellite on the high energy side of Co $2p_{3/2}$ confirms the existence of these Co^{2+} ions. Relatively low intensity satellites located in between Co $2p_{3/2}$ and Co $2p_{1/2}$ indicate that Co ions are present in a partial spinel-type lattice arrangement and these low intensities satellite could also indicate the presence of Co^{3+} ions mixing with Co^{2+} ions [6]. The asymmetry in the Co $2p_{1/2}$ peak confirms the existence of Co^{2+} and Co^{3+} ions.

The decoupling of the Co $2p_{3/2}$ peak and the satellite at the high energy side of this peak in every spectrum provides five curve-fitting components (Fig. 5. a-d). The peaks in the region lower than 779.8 eV are mostly due to Co^{3+} in octahedral coordination while the peaks around 780 eV are predominantly attributed to the mixed Co(II,III) bonding states. The peak with binding energy of Co $2p_{3/2}$ above 780.0 eV with a shake-up satellite is characteristic of Co^{2+} in tetrahedral coordination. The binding energy and the percentage of each component are tabulated in Table 4. It can be seen that, in all samples, the tetrahedral Co^{2+} ions dominate. Nonetheless, even though they are prominent in a copper-cobalt mixed-oxides system, these Co^{2+} ions are partially substituted by Cu^{2+} ions[8, 35] forming copper–cobalt oxide structures [6]. The increases of annealing temperatures between 500 to 650°C generally do not influence the cobalt bonding structure in the surface.

Fig. 6 shows the O *1s* XPS spectra and curve-fittings of copper cobalt oxide film coatings synthesized at different annealing temperatures. In every spectrum, the O *1s* exhibits a strong peak with a shoulder at its higher binding energy side. The decoupling of the O *1s*

photoelectron spectrum results in four curve-fittings grouped into three components. The component at binding energy around 529.3-529.4 eV (denoted "i") is attributed to lattice O^{2-} in the structure, while the components at BE around 530.4-531.5 eV (denoted "ii" and "iii") may be due to the surface oxygen from a wide variety of species such as chemisorbed oxygen O^-, oxygen containing surface contamination, and/or OH-like species, as hydroxyl, carbonate groups, *etc*. [6, 8, 18, 37-40]. The component at BE around 531.8-532.5 eV (denoted "iv") could be assigned to subsurface (bulk structure near surface) O^- species [41, 42]. The apparent shoulders at the high energy side of the O *1s* main peaks are the characteristic feature of the copper-cobalt mixed oxides family which distinguishes them from O *1s* on Co_3O_4 [8]. Overall, there is no change in the oxygen surface compositions when the surfaces are treated at different annealing temperatures from 500 to 650°C.

3.3. Optical properties

The optical properties of the copper cobalt thin film coatings are evaluated on the basis of absorptance (α) within the wavelength range of 0.3-2.7 μm. Absorptance is defined as a weighted fraction between absorbed radiation and incoming radiation. The absorptance of a thin film on a substrate can be determined in terms of reflectance as described by Duffie and Beckman [24]. Low spectral reflectance indicates high absorptance and *vice versa*. The reflectance spectra of all the thin film coatings on highly reflective aluminium substrates synthesized at different annealing temperatures, together with their corresponding solar absorptance values, are shown in Fig. 7a. The prepared coatings exhibit low to moderate reflectance with interference peaks (wavy curves) round about 1.0-1.2 μm and absorption edges around 1.5-1.7 μm. The spectra essentially form solar selective absorber curve profiles within UV-Vis-NIR wavelengths area. Similar phenomena of the presence of interference peaks and absorption edges have also been reported by others researchers [43, 44]. The increase in temperature generally tends to raise the interference peaks and the absorption edge positions that reduce the absorptance values. The sample annealed at 550°C is an exception as

the interference peak and the absorption edge approach each other leading to the smallest wavy curve amplitude and the highest absorptance value among the coatings (α = 84.4%). Significant increases of the interference peak and the absorption edge positions are indicated by the coatings synthesized at annealing temperatures of 600°C and 650°C that decrease the absorptance value up to about 8% compared to the maximum absorptance value (Fig. 7b).

From Fig. 7a, it can be seen that the more significant changes of reflectance spectra occur near the infrared (NIR) wavelength region (> 0.8 μm). The reflectance property of copper–cobalt oxide layer in the NIR wavelengths area is affected by at least three factors; (1) the thickness of film coating, (2) the intrinsic properties of coating material, and (3) the reflectivity property of the substrate. For coatings with similar thicknesses, the reflectance features showed in Fig. 7a are due to the combined factors of solar wavelengths absorptions/scattering by the coating material (intrinsic properties) and the back-reflections of the NIR radiations transmitted through the coating material by the highly reflective aluminium substrate. The increase of annealing temperature from 500 to 650°C enhances the crystallinity of the coating material that subsequently might increase the scattering by the larger crystallite, leading to the decrease of absorption by the coating.

The choice of substrate also has a substantial influence on the reflectance property of the coatings. It is widely accepted that the longer the NIR wavelength, the more radiation will be transmitted through the semiconductor coating material due to the smaller energy owned by the radiations/photons, which makes them easier to pass the coating material without being absorbed. This transmitted-through radiation will be then reflected back by the reflective substrate (dark mirror absorber-reflector tandem concept). In view of this, it seems that our coatings behave akin to a semiconductor material. The increase of annealing temperature, *i.e* more than 550°C in the coating synthesis process, might increase the intrinsic "band gap energy" of the coating. As such, the smaller number of the incident NIR photons are absorbed through the transition across the band gap, while more photons are transmitted through the

coating. This transmitted radiation will then be reflected back by the reflective substrate which eventually increases the reflectance and decreases the absorptance.

3.4. Nanoindentation tests

Fig. 8 shows representative load-displacement curves obtained from nanoindentation experiments on the thin film coatings treated at different annealing temperatures. From these curves the values of elastic modulus (*E*), hardness (*H*) of the thin films and their wear resistance index (*H/E*) are derived and presented in Fig. 9. From Fig. 8, the level of resistance to deformation of copper cobalt oxide thin film coatings increases with rising annealing temperature; the coating annealed at temperature 650°C exhibits the highest resistance to deformation. The elastic moduli of all the coatings are lower than that of the aluminium substrate, consistent with our previous findings [19]. In addition, the obtained hardness values of the present study are generally consistent with those reported by other researchers [45, 46]. Compared to the Young's modulus and hardness obtained on the similar samples [Cu]/[Co] = 0.3M/0.3M without heat treatment [21], the results in this work were slightly higher after annealing. Further, following heat treatment, there is an increasing trend in both elastic modulus and hardness for the coatings, albeit this is not so pronounced for hardness. Hence, it can be construed that the heat treatment exerts a positive impact on the mechanical properties of the coating layer. The spread of the measurement results, and the associated errors in both the modulus and hardness, may be due to the surface roughness and the porosity of the coatings [19, 20].

Wear resistance is vital to the performance and reliability of the optical coatings during service, where mechanical contacts are always expected. Previous studies indicated that the hardness to modulus ratio, *H/E*, is an important parameter for predicting the wear resistance [47]. Even though there is a decreased tendency in *H/E* ratio of the coatings with increasing annealing temperature, all coatings prepared in this work are envisaged to have superior wear resistance when compared with the aluminium substrate (Fig. 9(c)).

3.5. Finite Element Modelling (FEM)

FEM simulation was conducted using parameters listed in Table 5, in which the yield strength was estimated as H/3 [48]. The results for the coating annealed at 650°C are shown in Fig. 10, where the stress distribution under progressive loading is presented. Notably, the higher stress, as well as the associated plastic zone, was primarily concentrated within the coating layer, up to an indentation depth of 0.06 μm. For the loading conditions modelled, only about half of the maximum stress level could expand into the substrate. This is because all the coating layers have lower elastic modulus but higher hardness than those of the Anofol aluminium substrate (E_{Al} = 131.41 GPa, H_{Al} = 1.455 GPa), which were evaluated experimentally in our previous works [19 - 21]. Consequently, little plastic deformation would result within the Al substrate. Considering the fact that for all the samples, variations in both Young's modulus and Poisson's ratio only occur within a narrow range, contact-induced stress distributions in the other coatings are similar. Some variations, although not significant, were observed in the stress distributions (Fig. 10), compared to our previous work [21], due to the change in the mechanical properties of coatings after annealing at the temperature of 650 °C Therefore, two implications can be derived from the above analysis. a) Coating delamination would be suppressed, which typically occurs at the interface between the coating and *plastically* deformed substrate during unloading. It has been well established that delamination is a direct consequence of plastic deformation within the substrate [49, 50]. b) Mechanical damage, once induced, would be confined within the coating under moderate loading conditions. In contrast, when the same loading is applied directly onto the Al substrate, a marked difference can be observed in Fig. 11, where the plastic zones of the loaded samples (coated and uncoated) are determined from FEM results using domain integration and plotted against the indentation depth. The size of the plastic zone resulting from the same loading has increased by 5-7 times, indicating a significant increase in the plastic deformation. It is worth noting that the plastic deformation is detrimental to the

integrity of the coating/substrate system. While the plastic zone within the coating layer represents a damage mechanism which is undesirable and cannot be overlooked, the marked reduction of its size, compared to that in the bare substrate, signifies a distinct improvement in load bearing capability. From these results, improvement in the load-bearing performance is expected when applying to the Al substrate with a coating layer having higher *H/E*, such as the coatings being developed and studied here.

4. Conclusions

The copper-cobalt oxides thin film coatings were deposited on aluminium substrates and then treated at different annealing temperatures within the range 500-650°C. The resultant coatings were characterized *via* XRD, XPS, UV-Vis-NIR and nanoidentation methods. An increase in the mean size of the crystalline domains of the coatings was found with the increase of annealing temperature. The chemistry binding structures on the surface characterized by XPS remained relatively unaltered with the change in the annealing temperature up to 650 °C. The copper electronic structure consisted primarily of tetrahedral Cu^{+} in addition to octahedral Cu^{2+}. The cobalt electronic structure comprised tetrahedral Co^{2+} ions, octahedral Co^{3+} and mixed Co(II,III) oxidation states. The oxygen oxidation states consisted mainly of lattice O^{2-} with minor surface and subsurface oxygen. Optical properties characterized by UV-Vis-NIR revealed that the increase of the annealing temperature to 550°C increased the absorptance which reached the maximum value of α = 84.4%, while further increases of temperature decreased the absorptance. This transition was caused by the integrated effects of the intrinsic properties of coating material and the substrate surface optical properties. Mechanical properties measured by nanoindentation tests revealed that both the elastic modulus and the hardness had an increasing trend but there was a slight decrease in *H/E* ratio as the annealing temperature was increased. However, by using *H/E* as an indicator, the wear resistance of all these coating materials was expected to be superior to

that of the aluminium substrate. FEM modelling indicated that, under mechanical loading conditions, stress and plastic deformation were primarily concentrated within the coating layers. This would reduce the likelihood of delamination of the coating layer upon unloading.

Acknowledgements

We would like to acknowledge Mr. Ken Seymour for his assistance in sample preparation. Amun Amri and M. Mahbubur Rahman are highly grateful to the Indonesian Government and Murdoch University respectively, for providing PhD scholarship.

References

[1] K. Fujimoto, T. Oba, Applied Catalysis, 13 (1985) 289-293.

[2] J.E. Baker, R. Burch, S.E. Golunski, Applied Catalysis, 53 (1989) 279-297.

[3] X. Xiaoding, E.B.M. Doesburg, J.J.F. Scholten, Catalysis Today, 2 (1987) 125-170.

[4] S. Angelov, D. Mehandjiev, B. Piperov, V. Zarkov, A. Terlecki-Baricˇevic´, D. Jovanovic´, Z. Jovanovic´, Applied Catalysis, 16 (1985) 431-437.

[5] R. Bonchev, T. Zheleva, S.C. Sevov, Chemistry of Materials, 2 (1990) 93-95.

[6] J.L. Gautier, E. Trollund, E. Ríos, P. Nkeng, G. Poillerat, Journal of Electroanalytical Chemistry, 428 (1997) 47-56.

[7] B. Marsan, N. Fradette, G. Beaudoin, Journal of The Electrochemical Society, 139 (1992) 1889-1896.

[8] M. De Koninck, S.-C. Poirier, B. Marsan, Journal of The Electrochemical Society, 153 (2006) A2103-A2110.

[9] G. Fornasari, S. Gusi, F. Trifiro, A. Vaccari, Industrial & Engineering Chemistry Research, 26 (1987) 1500-1505.

[10] G.G. Volkova, T.A. Krieger, L.M. Plyasova, V.A. Zaikovskii, T.M. Yurieva, Copper-cobalt catalysts for higher alcohols synthesis from syngas, in: R.L.E.C.P.N.J.H.S. M. de Pontes, M.S. Scurrell (Eds.) Studies in Surface Science and Catalysis, Elsevier, 1997, pp. 67-72.

[11] G.G. Volkova, T.M. Yurieva, L.M. Plyasova, M.I. Naumova, V.I. Zaikovskii, Journal of Molecular Catalysis A: Chemical, 158 (2000) 389-393.

[12] D.J. Singh, Physical Review B, 76 (2007) 085110.

[13] M. Beekman, J. Salvador, X. Shi, G.S. Nolas, J. Yang, Journal of Alloys and Compounds, 489 (2010) 336-338.

[14] R.N. Singh, J.P. Pandey, N.K. Singh, B. Lal, P. Chartier, J.F. Koenig, Electrochimica Acta, 45 (2000) 1911-1919.

[15] M. Hamid, A.A. Tahir, M. Mazhar, K.C. Molloy, G. Kociok-Köhn, Inorganic Chemistry Communications, 11 (2008) 1159-1161.

[16] W.M. Shaheen, A.A. Ali, Materials Research Bulletin, 36 (2001) 1703-1716.

[17] R.D. Shannon, D.B. Rogers, C.T. Prewitt, J.L. Gillson, Inorganic Chemistry, 10 (1971) 723-727.

[18] A. La Rosa-Toro, R. Berenguer, C. Quijada, F. Montilla, E. Morallon, J.L. Vazquez, The Journal of Physical Chemistry B, 110 (2006) 24021-24029.

[19] A. Amri, Z.-T. Jiang, T. Pryor, C.-Y. Yin, Z. Xie, N. Mondinos, Surface and Coatings Technology, 207 (2012) 367-374.

[20] A. Amri, X. Duan, C.-Y. Yin, Z.-T. Jiang, M.M. Rahman, T. Pryor, Applied Surface Science, 275 (2013) 127-135.

[21] A. Amri, Z.-T. Jiang, P.A. Bahri, C.-Y. Yin, X. Zhao, Z. Xie, X. Duan, H. Widjaja, M.M. Rahman, T. Pryor, The Journal of Physical Chemistry C, 117 (2013) 16457-16467.

[22] M.S. Ahmed, X. Zhao, Z.-f. Zhou, P. Munroe, N. Chen-Tan, L.K.Y. Li, Z. Xie, Journal of the American Ceramic Society, 94 (2011) 1546-1551.

[23] M.S. Ahmed, P. Munroe, Z.-T. Jiang, X. Zhao, M. Wajrak, H. Guo, W. Rickard, Z. Xie, Journal of the American Ceramic Society, 95 (2012) 2997-3004.

[24] J.A. Duffie, W.A. Beckman, Solar Engineering of Thermal Processes, third ed., John Wiley & Sons Inc., New Jersey, 2006.

[25] M.S. Ahmed, Z.-f. Zhou, P. Munroe, L.K.Y. Li, Z. Xie, Thin Solid Films, 519 (2011) 5007-5012.

[26] W.C. Oliver, G.M. Pharr, Journal of Materials Research, 19 (2004) 3-20.

[27] X. Zhao, Z. Xie, P. Munroe, Materials Science and Engineering: A, 528 (2011) 1111-1116.

[28] Z. Li, P. Munroe, Z.-t. Jiang, X. Zhao, J. Xu, Z.-f. Zhou, J.-q. Jiang, F. Fang, Z.-h. Xie, Acta Materialia, 60 (2012) 5735-5744.

[29] H.P. Klug, L.E. Alexander, X-Ray Diffraction Procedures: For Polycrystalline and Amorphous Materials, 2nd Edition, by Harold P. Klug, Leroy E. Alexander, pp. 992. ISBN 0-471-49369-4. Wiley-VCH, May 1974., 1 (1974).

[30] B. Heying, X. Wu, S. Keller, Y. Li, D. Kapolnek, B. Keller, S.P. DenBaars, J. Speck, Applied Physics Letters, 68 (1996) 643-645.

[31] H. Uwe, G. Neil, Nature Nanotechnology, 6 (2011) 534-534.

[32] I.C. Noyan, J.B. Cohen, Residual stresses: measurement by diffraction and interpretation; with 31 tables, SPRINGER VERLAG GMBH, 1987.

[33] L.B. Freund, S. Suresh, Thin Film Materials: Stress, Defect Formation and Surface Evolution, Cambridge University Press, 2003.

[34] A.P. Boresi, R.J. Schmidt, Advanced mechanics of materials, John Wiley & Sons, 2003.

[35] R. Amadelli, L. Samiolo, A. Maldotti, A. Molinari, M. Valigi, D. Gazzoli, International Journal of Photoenergy, 2008 (2008).

[36] G. Fierro, M. Lo Jacono, M. Inversi, R. Dragone, P. Porta, Topics in Catalysis, 10 (2000) 39-48.

[37] T.J. Chuang, C.R. Brundle, D.W. Rice, Surface Science, 59 (1976) 413-429.

[38] G. Tyuliev, D. Panayotov, I. Avramova, D. Stoichev, T. Marinova, Materials Science and Engineering: C, 23 (2003) 117-121.

[39] P. Stefanov, I. Avramova, D. Stoichev, N. Radic, B. Grbic, T. Marinova, Applied Surface Science, 245 (2005) 65-72.

[40] G. Tyuliev, S. Angelov, Applied Surface Science, 32 (1988) 381-391.

[41] J.-C. Dupin, D. Gonbeau, P. Vinatier, A. Levasseur, Physical Chemistry Chemical Physics, 2 (2000) 1319-1324.

[42] S. Royer, A. Van Neste, R. Davidson, S. Mcintyre, S. Kaliaguine, Industrial & engineering chemistry research, 43 (2004) 5670-5680.

[43] T. Bostrom, E. Wackelgard, G. Westin, Solar Energy, 74 (2003) 497-503.

[44] R. Bayón, G. San Vicente, C. Maffiotte, Á. Morales, Renewable Energy, 33 (2008) 348-353.

[45] W. Que, Z. Sun, Y. Zhou, Y.L. Lam, S.D. Cheng, Y.C. Chan, C.H. Kam, Materials Letters, 42 (2000) 326-330.

[46] C.M. Chan, G.Z. Cao, H. Fong, M. Sarikaya, T. Robinson, L. Nelson, Journal of Materials Research, 15 (2000) 148-154.

[47] A. Leyland, A. Matthews, Wear, 246 (2000) 1-11.

[48] B.R. Lawn, R.F. Cook, Journal of Materials Science, 47 (2012) 1–22.

[49] M.T. Tilbrook, D.J. Paton, Z. Xie, M. Hoffman, Acta Materialia, 55 (2007) 2489-2501.

[50] R.K. Singh, M.T. Tilbrook, Z.H. Xie, A. Bendavid, P.J. Martin, P. Munroe, M. Hoffman, Journal of Materials Research, 23 (2008) 27-36.

Table 1. Results of grain/domain size derived using Debye-Scherrer formula from the (3 1 0) and (3 0 1) lattice planes.

Annealing Temperatures (^{o}C)	Domain size (nm)	
	(310) plane	(301) plane
500	26	221
550	53	252
600	61	196
650	101	196

Table 2. Residual stress within the $CoCu_2O_3$ phase, estimated by using the (310) and (301) peak position data from the X-ray diffraction

Annealing temperature (°C)	2θ for (310) peak	2θ for (301) peak	Tensile residual stress, σ_x (GPa)
500	36.920	40.354	0.65
550	36.990	40.324	0.65
600	36.920	40.252	0.48
650	36.860	40.191	0.34
Reference	36.445	40.243	0.00

Table 3. The curve-fittings results of Cu $2p_{3/2}$ and its satellite of copper cobalt film coatings synthesized at different annealing temperatures.

Annealing temperature	Binding energy and percentage			
	Cu $2p_{3/2}$ photoelectron line		Satellite I	Satellite II
500 °C	932.3 eV (43.7 %)	933.5 eV (38.0 %)	940.5 eV (9.4 %)	943.0 eV (8.9 %)
550 °C	932.3 eV (42.9 %)	933.5 eV (38.9 %)	940.6 eV (10.3 %)	943.1 eV (7.9 %)
600 °C	932.3 eV (47.1 %)	933.5 eV (36.2 %)	940.6 eV (8.1 %)	943.1 eV (8.6 %)
650 °C	932.4 eV (47.5%)	933.5 eV (37.4 %)	940.6 eV (7.4 %)	943.2 eV (7.7 %)
Attributions:	Tetrahedral Cu^{+}	Octahedral Cu^{2+}	Cu^{2+} characteristic satellites	

Table 4. The curve-fittings results of Co $2p_{3/2}$ and its satellite of copper cobalt film coatings synthesized at different annealing temperatures.

Annealing temperature	Binding energy and percentage				
	Co $2p_{3/2}$ photoelectron line			satellites	
	i	ii	iii	iv	v
500°C	779.0 eV (13.3 %)	780.0 eV (27.5 %)	781.9 eV (31.7 %)	785.7 eV (15.1 %)	787.7 eV (12.4 %)
550°C	778.9 eV (10.6 %)	779.9 eV (24.6 %)	781.7 eV (35.9 %)	785.5 eV (13.3 %)	787.6 eV (15.6 %)
600°C	778.9 eV (9.24 %)	779.8 eV (27.7 %)	781.7 eV (34.5 %)	785.6 eV (14.8 %)	787.9 eV (13.7 %)
650°C	778.9 eV (11.1 %)	779.9 eV (26.1 %)	781.6 eV (34.8 %)	786.0 eV (22.7 %)	789.3 eV (5.3 %)
Attributions	Octahedral Co(III)	Co(II,III)	Tetrahedral Co(II)	Co(II) characteristic satellites	

Table 5. Mechanical parameters derived from the nanoindentation and used for FEM modelling

Parameters	Temperatures (°C)			
	500	550	600	650
E (GPa)	91.4	101.4	101.5	105.1
H(GPa)	3.18	3.20	3.22	3.17
H/E	0.035	0.032	0.032	0.030
Yield strength (σ_y) (GPa)	1.06	1.07	1.07	1.06
Poisson's ratio	0.3	0.3	0.3	0.3

List of Figure Captions

Fig. 1. XRD patterns of the prepared copper–cobalt thin film coatings on aluminum substrate at different annealing temperatures.

Fig.2. Cu *2p* XPS spectra of copper cobalt thin film coatings synthesized at different annealing temperatures.

Fig.3. Decoupling of Cu $2p_{3/2}$ peaks of copper cobalt thin film coatings synthesized at different annealing temperatures.

Fig.4. Co *2p* XPS spectra of copper cobalt thin film coatings synthesized at different annealing temperatures.

Fig.5. Decoupling of Co $2p_{3/2}$ peaks of copper cobalt thin film coatings synthesized at different annealing temperatures.

Fig.6. O *1s* XPS spectra and curve-fittings of copper cobalt thin film coatings synthesized at different annealing temperatures.

Fig.7. Reflectance spectra and solar absorptance of copper–cobalt oxide thin film coatings on aluminium substrates synthesized at different annealing temperatures (a), Absorptance *versus* annealing temperature (b).

Fig.8. Typical load-displacement curves obtained from coatings treated at different annealing temperatures.

Fig.9. Mechanical properties of the as-deposited coatings derived from the nanoindentation tests, (a) elastic modulus, (b) hardness, and (c) *H/E*. The wear resistance index of aluminium are also displayed for comparison purpose.[19]

Fig.10. Stress distribution of coating treated at annealing temperature of 650°C, obtained from FEM simulations for different indentation depths: (a) 0.03 μm, (b) 0.04 μm, (c) 0.05 μm,

and (d) 0.06 μm. The dark lines close to the bottom of each model represent the interface between the coating and the substrate.

Fig.11. Variations of the plastic zone size in coatings synthesized at annealing temperatures of 500-650°C compared to the aluminium under increasing load, derived from domain integration of the FEM results.

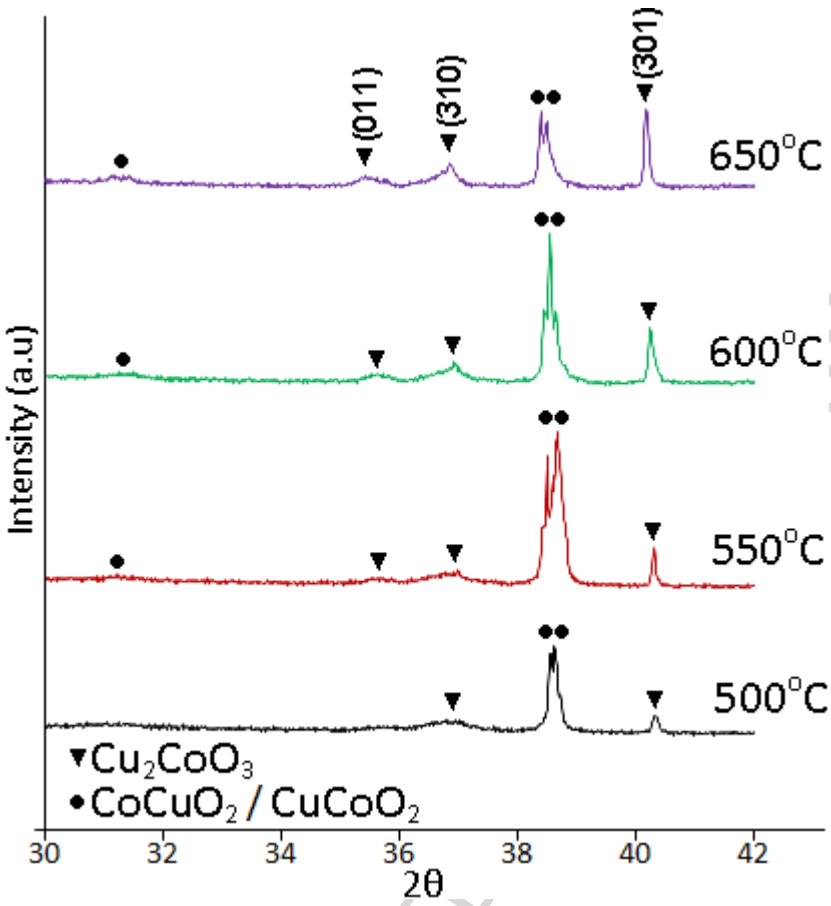

Fig. 1.

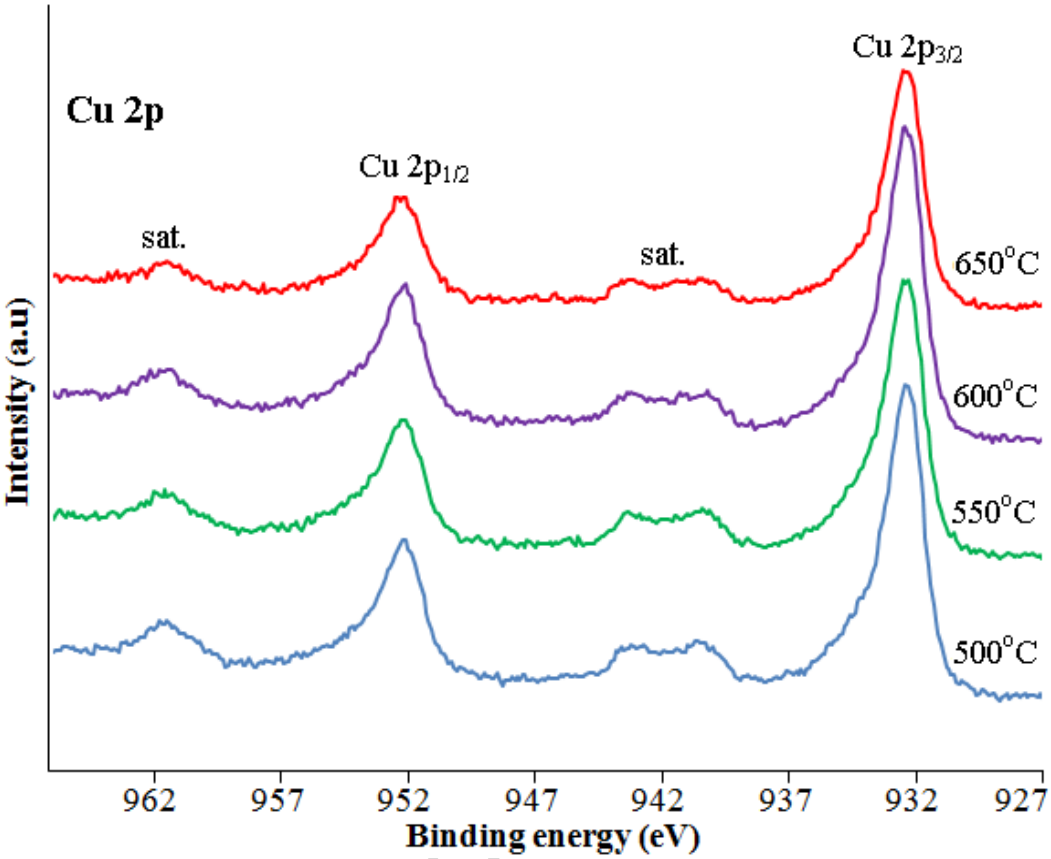

Fig. 2.

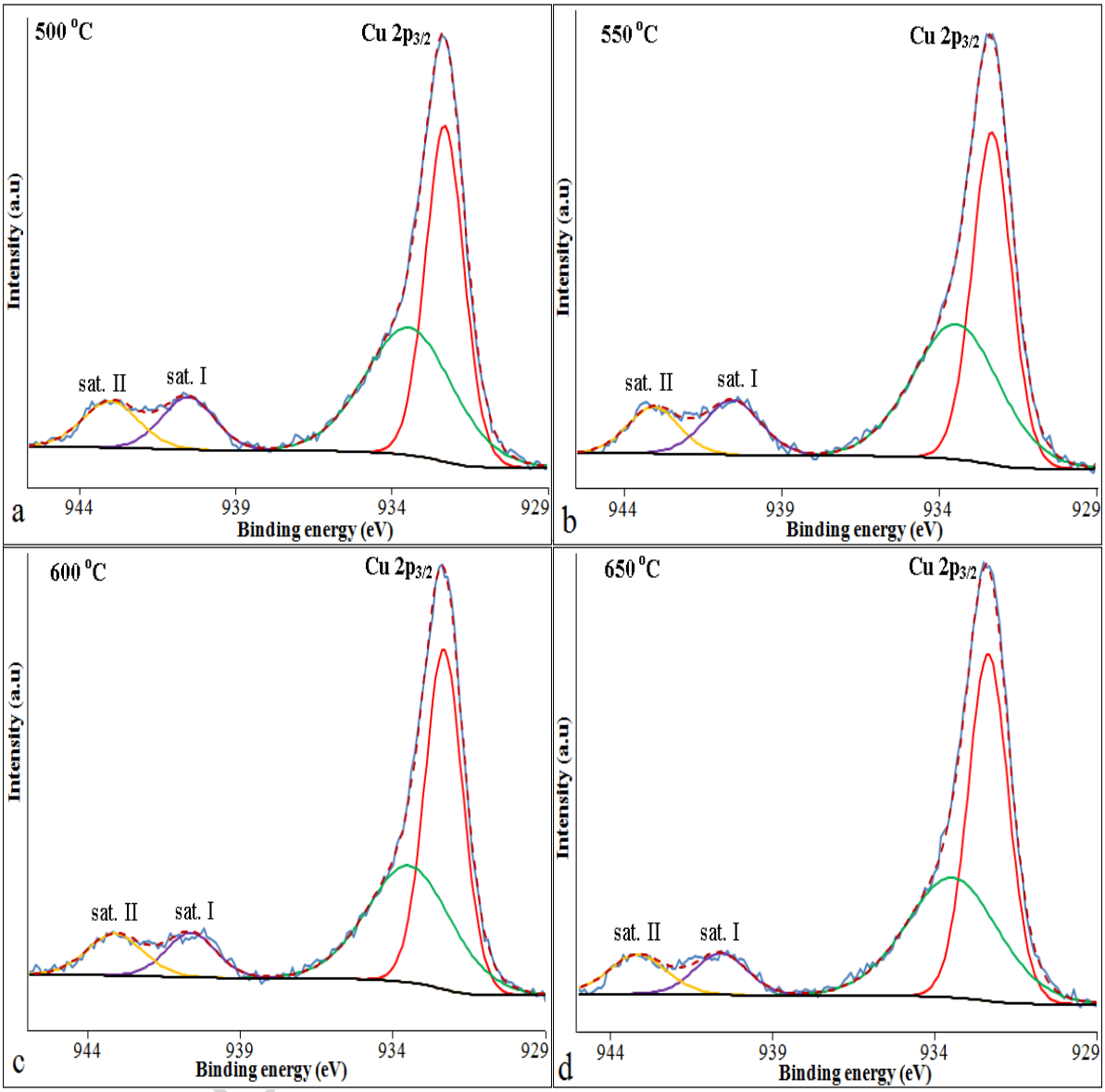

Fig. 3.

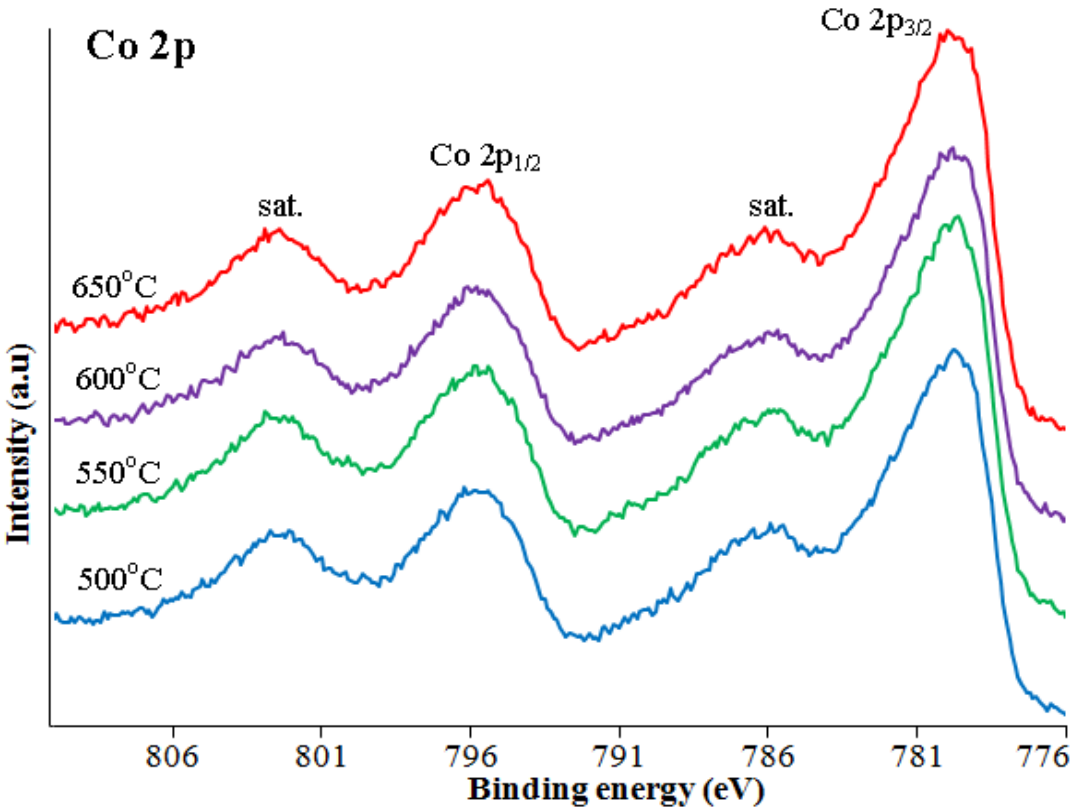

Fig. 4.

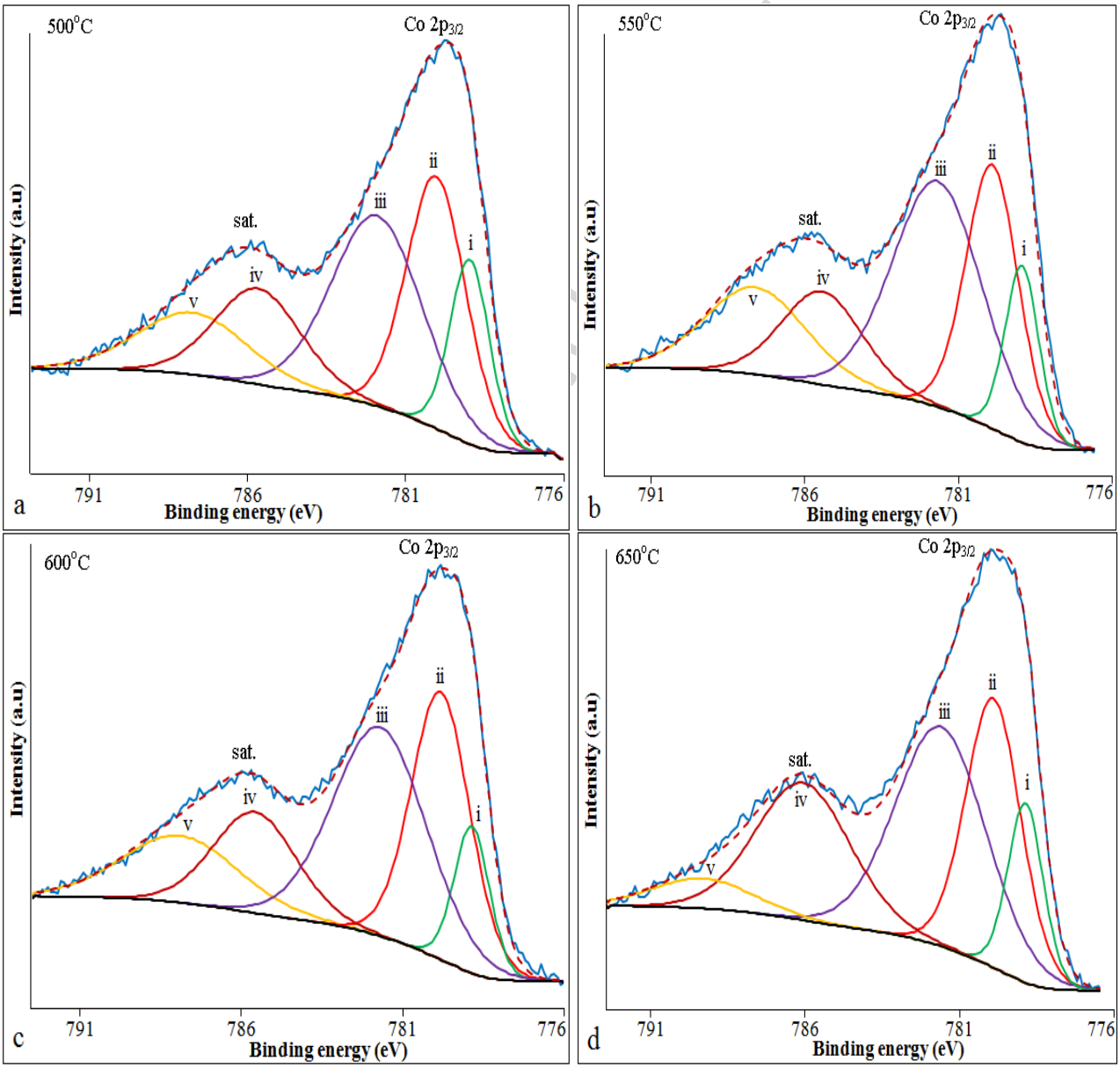

Fig. 5.

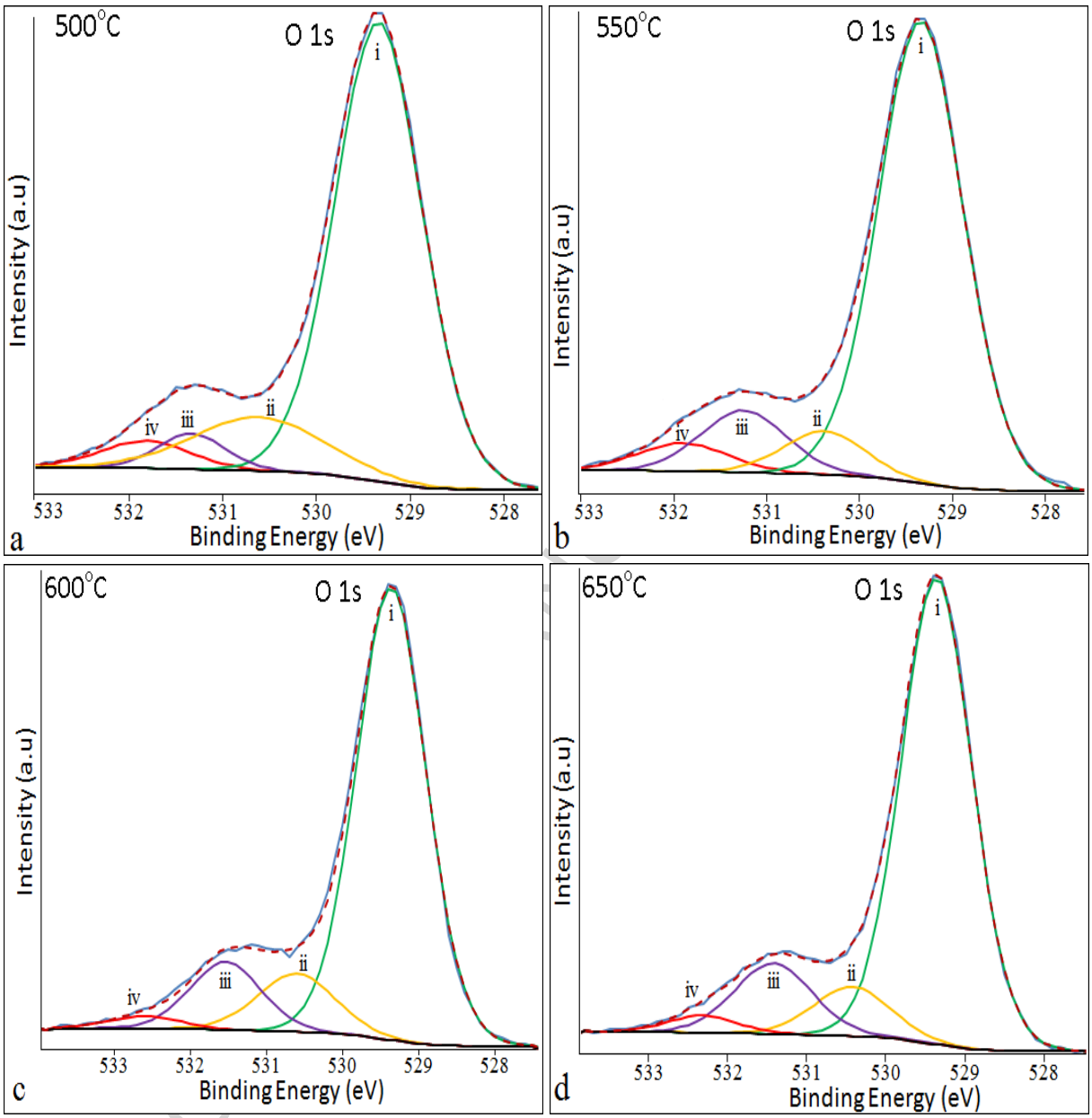

Fig. 6.

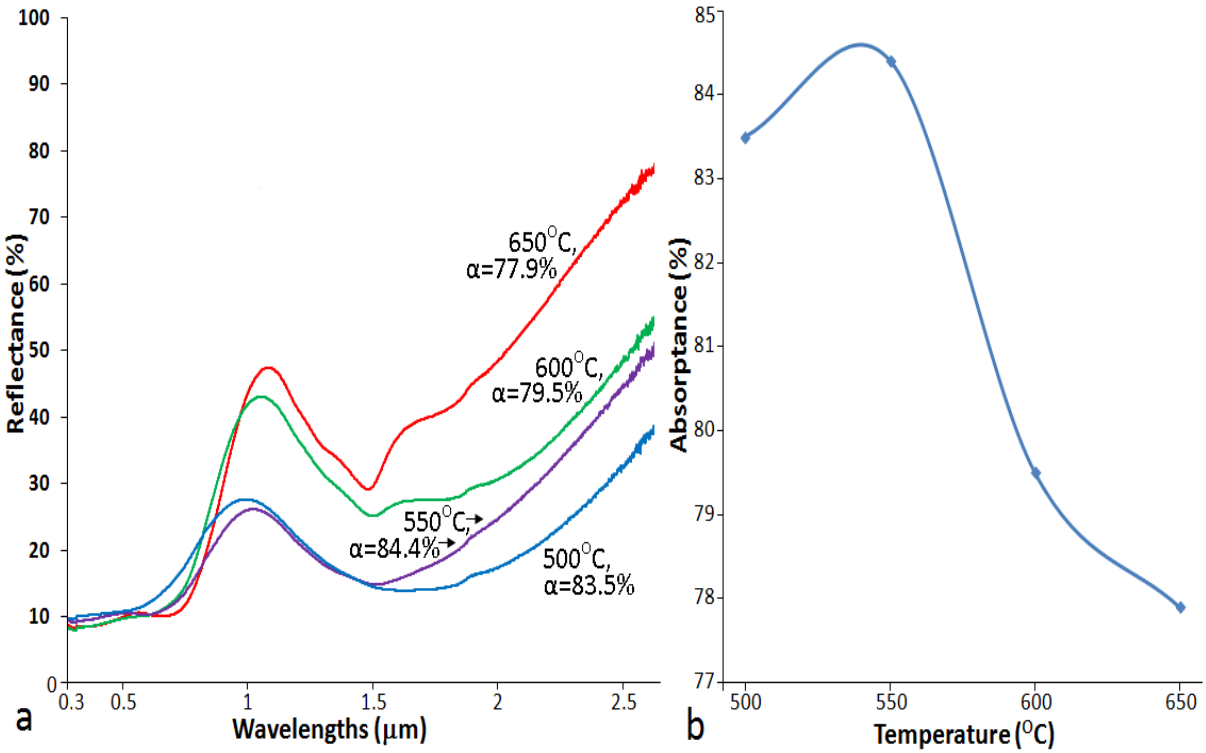

Fig. 7.(a)(b)

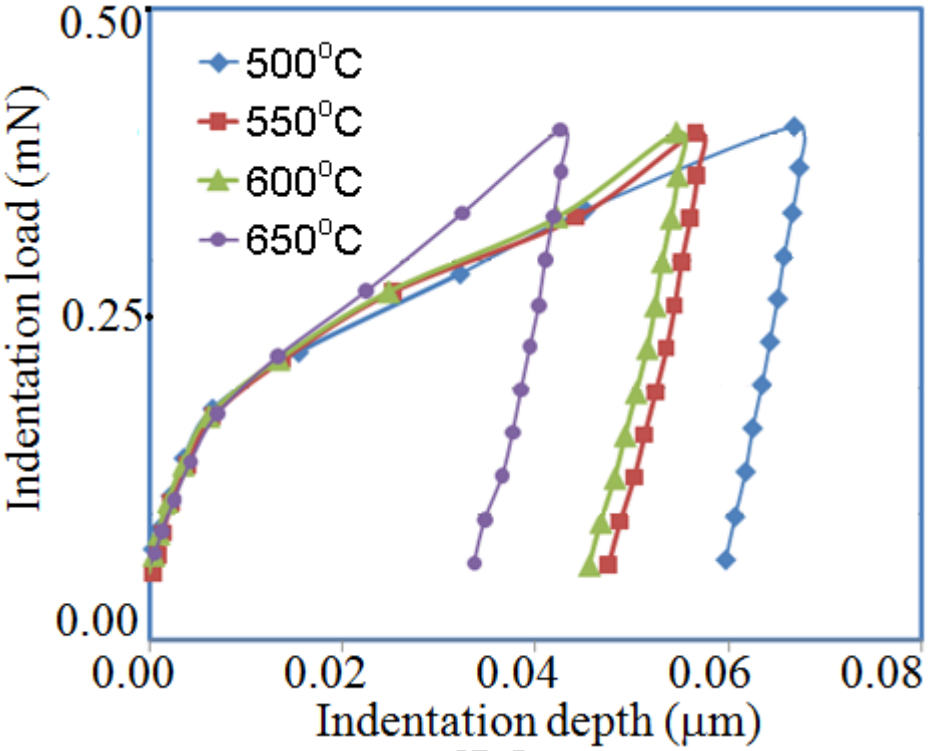

Fig. 8.

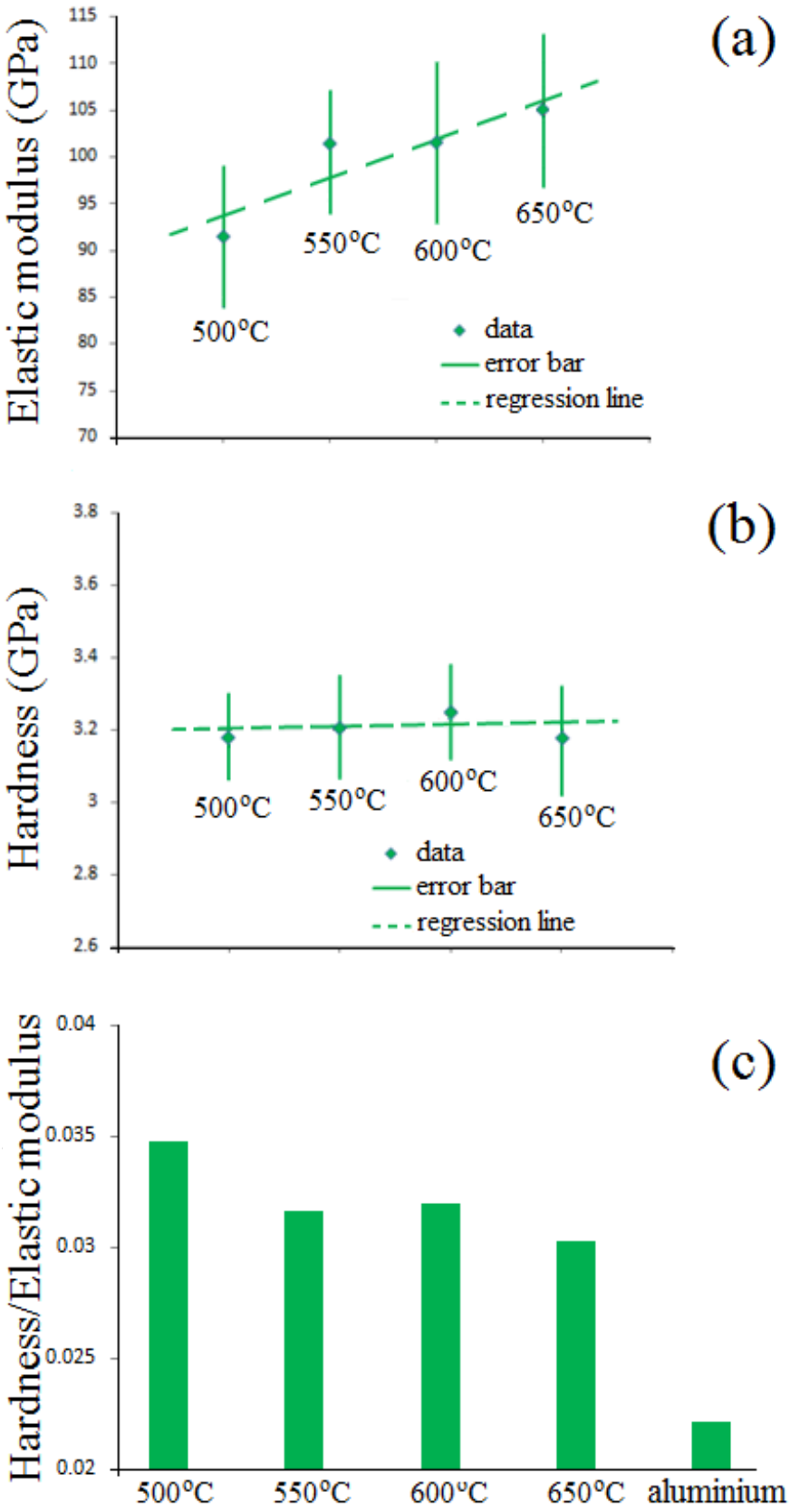

Fig. 9.

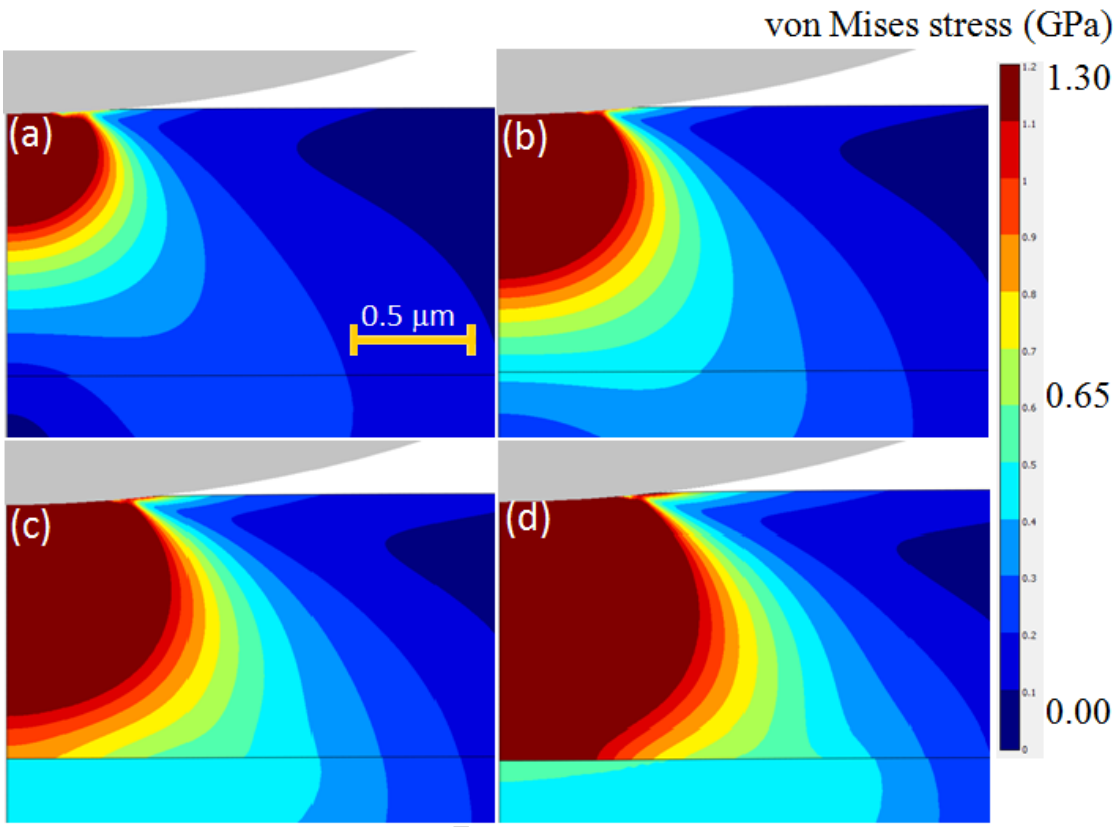

Fig. 10

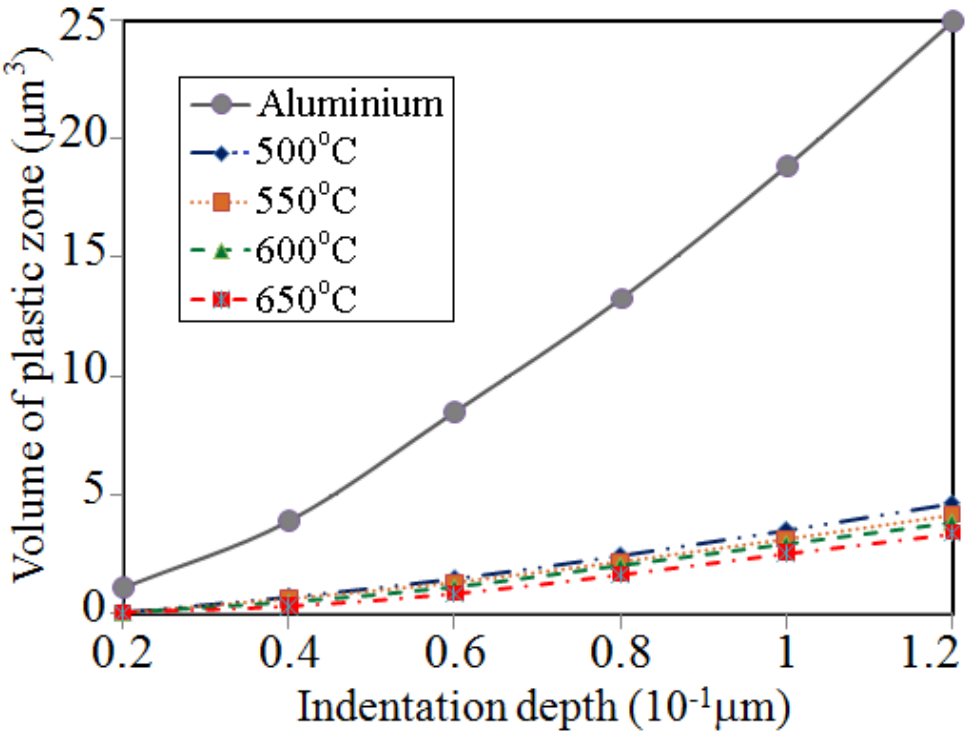

Fig. 11.

Research Highlights

> Copper-cobalt oxides are coated on aluminium substrates *via* sol-gel technique. > Tetrahedral Cu^{+}, octahedral Cu^{2+}, tetrahedral Co^{2+} ions and octahedral Co^{3+} are detected. > Increase of the annealing temperature to 550°C increases the absorptance. > The maximum value of $\alpha = 84.4\%$ is obtained. > Stress and plastic deformation are concentrated within the coating layers.